

Adaptive Numerical Simulation of the Remediation of Soil Contamination by In-Situ Gas Venting

Victoria Pennington Peter K. Jimack
School of Computer Studies, University of Leeds

Abstract

This paper describes a mathematical model and adaptive numerical simulation of the time-dependent multiphase, multicomponent flow which occurs when a gas venting process is used to remove a volatile contaminant from a porous medium. The numerical simulation is adaptive in both space and time and involves the use of a finite element spatial discretization method incorporated within the SPRINT2D PDE software ([1]).

1 Introduction

An important environmental problem faced in a number of industrial sectors today is that of how to deal with the contamination of soil and groundwater due to spills or seepage of unwanted substances, such as chemical waste or hydrocarbons for example. Frequently these contaminants are volatile and will evaporate freely given a sufficient supply of unsaturated air. In such situations a popular clean-up technique is to employ a venting process which extracts the contaminant-rich gas phase by means of vacuum aspiration of the ground in the vicinity of the spill.

In this paper we consider a realistic multiphase porous media model for the extraction of a volatile contaminant (such as that resulting from a hydrocarbon spill), and present a stable, adaptive, finite element algorithm for the time-accurate solution of such a problem in two dimensions. Section 2 briefly describes the multiphase model, which consists of the equations of motion and associated domain and boundary conditions, whilst Sections 3 and 4 respectively discuss our adaptive discretization techniques and present some provisional numerical results.

2 Mathematical model

In the model problem considered here it is assumed that a hydrocarbon liquid has been spilled on ‘dry’ (unsaturated) ground, resulting in a volume distribution of this oleic liquid at or marginally above residual saturation throughout the vadose zone beneath the spill. For simplicity, it is assumed that the contaminant liquid has just two components, one volatile and water-soluble (referred to as *light oil* — component l) and one non-volatile and insoluble (*heavy oil* — component h). The other components present in the model are air (a) and water (w). The water is assumed to be non-volatile. There are four phases: a gas phase (g) consisting of light oil vapour and air; an oleic phase (o) consisting of light and heavy oils; an aqueous (water) phase (w) consisting of water and dissolved light oil; and a sorbed phase (s), being light and heavy oil sorbed to the soil surface. It is also assumed that when the venting process begins the spill has already occurred, resulting in a uniform distribution of the oleic phase at residual saturation; and that thermodynamic equilibrium exists between all phases.

The assumptions of residual saturations of the liquid phases mean that we can take both liquid phases to be immobile. Hence, in the equations of motion for the four components,

only the ones for the light oil and the air will involve convective terms (the sorbed phase being immobile by definition). These equations may be expressed as follows.

$$\frac{\partial}{\partial t}(\varepsilon\rho_g\alpha_g X_{lg} + \varepsilon\rho_o\alpha_o X_{lo} + \varepsilon\rho_w\alpha_w X_{lw} + c_s X_{ls}) + \nabla \cdot (\rho_g X_{lg} \underline{q}) = \nabla \cdot (\varepsilon\rho_g\alpha_g \mathbf{D}_{lg} \nabla X_{lg} + \varepsilon\rho_o\alpha_o \mathbf{D}_{lo} \nabla X_{lo} + \varepsilon\rho_w\alpha_w \mathbf{D}_{lw} \nabla X_{lw}) + S_l, \quad (2.1)$$

$$\frac{\partial}{\partial t}(\varepsilon\rho_o\alpha_o X_{ho} + c_s X_{hs}) = \nabla \cdot (\varepsilon\rho_o\alpha_o \mathbf{D}_{ho} \nabla X_{ho}), \quad (2.2)$$

$$\frac{\partial}{\partial t}(\varepsilon\rho_g\alpha_g X_{ag}) + \nabla \cdot (\rho_g X_{ag} \underline{q}) = \nabla \cdot (\varepsilon\rho_g\alpha_g \mathbf{D}_{ag} \nabla X_{ag}) + S_a, \quad (2.3)$$

$$\frac{\partial}{\partial t}(\varepsilon\rho_w\alpha_w X_{ww}) = \nabla \cdot (\varepsilon\rho_w\alpha_w \mathbf{D}_{ww} \nabla X_{ww}). \quad (2.4)$$

Here α_g is the pore-space volume fraction of the gas phase, ρ_g is the density of the gas phase, and X_{lg} is the mass fraction of light oil in the gas phase; similarly for all other components and phases. c_s denotes the total mass per unit volume porous medium that is sorbed to the soil surface, \underline{q} is the usual Darcy velocity (for the gas phase), \mathbf{D}_{lg} is the dispersivity tensor for light oil in the gas phase (and similarly for the other components and phases), and the functions S_l and S_a are source terms representing extraction of light oil vapour and air respectively.

Further details of the model may be found in [5] (or see [2] for a more comprehensive overview of this type of model), along with a description of a number of additional physical relations and constraints that must also hold. Using these additional relations it is possible to view the above system as one involving just four primary variables, which we choose to be X_{lg} , ρ_g , α_w and α_o respectively. All of the other variables present in equations (2.1) to (2.4) may be expressed in terms of these primary variables.

The numerical simulations described in this work all involve the use of a single vent which means that gas is extracted from just one point or line within the vadose layer. Fig. 1 illustrates a typical spatial domain (with boundary conditions) in which it has been assumed that the vent is positioned beneath the centre of an impermeable cover. At the free surface, where the soil is assumed to be open to the atmosphere, the boundary conditions must permit a non-zero flux (in *either* direction) of both gas phase components. We choose to model this, perhaps rather crudely, by applying Dirichlet conditions on X_{lg} and ρ_g at this part of the domain boundary. As has already been indicated, initial conditions are taken to be such that there has been a spillage of heavy and light oil mixture, resulting in a residual saturation (10% by volume say) of the liquid oil mixture, along with an already present 10% volume saturation of the liquid water. Conditions of thermodynamic equilibrium between the four phases and hydrostatic equilibrium in the gas phase are also assumed, and the gas extraction rate is initially zero (being increased to its full value over a start-up period of 1 second for example).

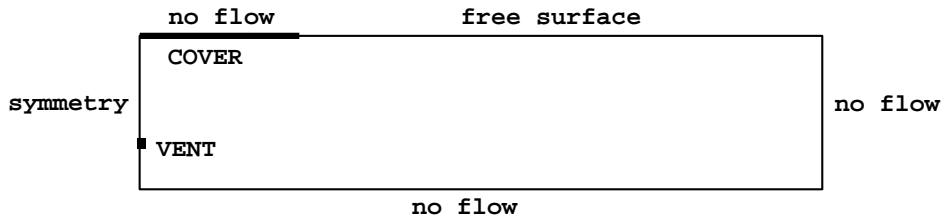


Figure 1: Test problem solution domain

3 Numerical method

For the numerical solution of the problem we employ the SPRINT2D adaptive PDE solver (see [1] for example). SPRINT2D uses the Method of Lines in which each of the PDEs are first discretized in space, resulting in a system of differential-algebraic equations which are then integrated in time using a DAE solver. SPRINT2D is a modular package which allows the use of a range of spatial discretization schemes for the solution of a large variety of problems. This is achieved by allowing the user of the software to write their own routine for calculating the residual vector for their particular discretization of the target problem. Each time this routine is called, a vector of solution values and corresponding time derivative values are passed in and a vector of residuals must be returned.

In this section we describe some details of the finite element discretization used in conjunction with SPRINT2D. Given a particular triangulation of the spatial domain we seek a piecewise linear approximation to each of the primary variables X_{lg} , ρ_g , α_w and α_o . This is achieved by first expressing equations (2.1) to (2.4) in a weak form and then replacing the arbitrary test functions by the usual piecewise linear ‘hat’ basis functions, N_j say. For example, the weak form of (2.1) is

$$\begin{aligned}
0 &= \int_{\Omega} \varepsilon(\rho_g \alpha_g \dot{X}_{lg} + \rho_g \dot{\alpha}_g X_{lg} + \dot{\rho}_g \alpha_g X_{lg}) W d\Omega \\
&+ \int_{\Omega} \varepsilon \rho_w (\alpha_w \dot{X}_{lw} + \dot{\alpha}_w X_{lw}) W d\Omega + \int_{\Omega} \varepsilon \rho_o (\alpha_o \dot{X}_{lo} + \dot{\alpha}_o X_{lo}) W d\Omega \\
&+ \int_{\Omega} (c_s \dot{X}_{ls} + \dot{c}_s X_{ls}) W d\Omega \\
&- \int_{\Omega} \rho_g X_{lg} \underline{q} \cdot \underline{\nabla} W d\Omega + \oint_{\Gamma} \rho_g X_{lg} \underline{q} \cdot \underline{n} W d\Gamma \\
&+ \int_{\Omega} \varepsilon \alpha_g \rho_g (\mathbf{D}_{lg} \underline{\nabla} X_{lg}) \cdot \underline{\nabla} W d\Omega - \oint_{\Gamma} \varepsilon \alpha_g \rho_g (\mathbf{D}_{lg} \underline{\nabla} X_{lg}) \cdot \underline{n} W d\Gamma \\
&+ \int_{\Omega} \varepsilon \alpha_o \rho_o (\mathbf{D}_{lo} \underline{\nabla} X_{lo}) \cdot \underline{\nabla} W d\Omega - \oint_{\Gamma} \varepsilon \alpha_o \rho_o (\mathbf{D}_{lo} \underline{\nabla} X_{lo}) \cdot \underline{n} W d\Gamma \\
&+ \int_{\Omega} \varepsilon \alpha_w \rho_w (\mathbf{D}_{lw} \underline{\nabla} X_{lw}) \cdot \underline{\nabla} W d\Omega - \oint_{\Gamma} \varepsilon \alpha_w \rho_w (\mathbf{D}_{lw} \underline{\nabla} X_{lw}) \cdot \underline{n} W d\Gamma \\
&+ \int_{\Omega} X_{lg} e \delta(\underline{x}) W d\Omega, \tag{3.1}
\end{aligned}$$

where Γ is the boundary of the domain Ω , the dot above a variable implies differentiation in time, and this equation is assumed to hold for all suitable test functions W . Also note that the source term S_l has been expressed in terms of a total gas extraction rate e and a Dirac delta function δ . In the Galerkin finite element method this weak form now becomes

$$\begin{aligned}
0 &= \sum_{e=1}^{n_e} \left[\int_{\Omega_e} \varepsilon (\tilde{\rho}_g \tilde{\alpha}_g \dot{\tilde{X}}_{lg} + \tilde{\rho}_g \dot{\tilde{\alpha}}_g \tilde{X}_{lg} + \dot{\tilde{\rho}}_g \tilde{\alpha}_g \tilde{X}_{lg}) N_j d\Omega \right. \\
&+ \int_{\Omega_e} \varepsilon \rho_w (\tilde{\alpha}_w \dot{\tilde{X}}_{lw} + \dot{\tilde{\alpha}}_w \tilde{X}_{lw}) N_j d\Omega + \int_{\Omega_e} \varepsilon \rho_o (\tilde{\alpha}_o \dot{\tilde{X}}_{lo} + \dot{\tilde{\alpha}}_o \tilde{X}_{lo}) N_j d\Omega \\
&+ \int_{\Omega_e} (\tilde{c}_s \dot{\tilde{X}}_{ls} + \dot{\tilde{c}}_s \tilde{X}_{ls}) N_j d\Omega - \int_{\Omega_e} \tilde{\rho}_g \tilde{X}_{lg} \tilde{\underline{q}} \cdot \underline{\nabla} N_j d\Omega \\
&+ \int_{\Omega_e} \varepsilon \tilde{\alpha}_g \tilde{\rho}_g (\tilde{\mathbf{D}}_{lg} \underline{\nabla} \tilde{X}_{lg}) \cdot \underline{\nabla} N_j d\Omega + \int_{\Omega_e} \varepsilon \tilde{\alpha}_o \rho_o (\tilde{\mathbf{D}}_{lo} \underline{\nabla} \tilde{X}_{lo}) \cdot \underline{\nabla} N_j d\Omega \\
&\left. + \int_{\Omega_e} \varepsilon \tilde{\alpha}_w \rho_w (\tilde{\mathbf{D}}_{lw} \underline{\nabla} \tilde{X}_{lw}) \cdot \underline{\nabla} N_j + \int_{\Omega_e} \tilde{X}_{lg} e \delta(\underline{x}) N_j d\Omega \right], \tag{3.2}
\end{aligned}$$

for each node j which is not on the free surface (a Dirichlet condition is applied to X_{lg} at those nodes on the free-surface). In the above we have followed the usual finite element convention of expressing all of the integrals as sums of integrals over each of the elements in the triangulation. The use of the tilde symbol above each variable has been used to indicate that this is the approximate form of that variable derived from a piecewise linear representation of the four primary variables and their time derivatives. Similar systems of finite element equations may be derived for (2.2), (2.3) and (2.4): see [5] for full details.

The mathematical model described in Section 2 clearly involves convective terms, with strengths depending significantly upon the rate of gas extraction at the vent. It is well known that centred discretization schemes, such as the Galerkin method, are prone to numerical instabilities in such situations (see [3] for example) and these may be observed in the region of the vent for the above discretization even when the extraction rate, e , is quite small (see Section 4 for typical values). Furthermore, refinement of the finite element mesh in the regions of difficulty merely serves to delay the onset of this instability.

General Petrov-Galerkin methods (such as [4, 6] for example) do exist for obtaining stable finite element discretizations in just these circumstances, however we prefer to follow the observation of Forsyth and Shao in [3], that it is only necessary to modify the evaluation of the convective terms $\underline{\nabla} \cdot (\rho_g X_{lg} \underline{q})$ and $\underline{\nabla} \cdot (\rho_g X_{ag} \underline{q})$ in equations (2.1) and (2.3) respectively. This modification simply requires the use of upstream values for X_{lg} , X_{ag} and ρ_g (but not necessarily \underline{q}) in these terms. For example, when using a three point quadrature rule, instead of taking the values of X_{lg} , X_{ag} and ρ_g at the midpoints of each edge to be the arithmetic average of the values at the two end points, we now take a one-sided average based upon the pressure difference along the edge. This may be viewed as modifying the quadrature rule to a vertex-based rule as illustrated in Fig. 2. Although this rule may be of lower order it leads to a more stable discretization when the pressure difference along an edge is large.

The use of adaptivity in both space and time allows the solver to apply most computational effort in the regions of the domain which most require it. Adaptivity in time is automatically controlled from within SPRINT2D so as to allow time-accuracy based upon local error estimates. The adaptivity in space is based upon hierarchical h-refinement (and coarsening) and is controlled by a user-supplied error indicator (or *a posteriori* error estimate if available). All of the computations described in Section 4 below were based upon the use

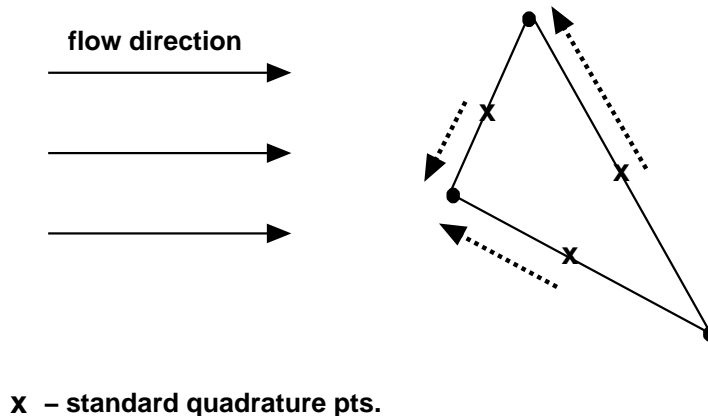


Figure 2: Illustration of quadrature point shifts used in the upstream method

of the following anisotropic error indicator on each element Ω_e :

$$\begin{aligned} err(\Omega_e) = \text{area}(\Omega_e) & \left[w_1 \left(\left| \frac{\partial X_{lg}}{\partial x} \right| + \left| \frac{\partial X_{lg}}{\partial y} \right| \right) + w_2 \left(\left| \frac{\partial \rho_g}{\partial x} \right| + \left| \frac{\partial \rho_g}{\partial y} \right| \right) + \right. \\ & \left. w_3 \left(\left| \frac{\partial \alpha_w}{\partial x} \right| + \left| \frac{\partial \alpha_w}{\partial y} \right| \right) + w_4 \left(\left| \frac{\partial \alpha_o}{\partial x} \right| + \left| \frac{\partial \alpha_o}{\partial y} \right| \right) \right], \end{aligned} \quad (3.3)$$

with weight vector $\underline{w} = (2.5, 1.25, 0.0, 0.0)^T$, and a target value of 0.025 on each element.

4 Results

In this section we present a small number of sample results for a test problem involving a symmetric $3\text{m} \times 15\text{m}$ domain which has an impermeable cover of radius 3m on the ground surface above a vent positioned 2m below the surface (again see Fig. 1). The particular spillage being modeled is that of n-Dodecane and Toluene (heavy and light oils respectively) and the chosen gas extraction rate is 0.01 kg/s (exhaustive details of all parameters and physical constants may be found in [5]). The initial mesh is very coarse throughout (just 16 by 4 mesh points) other than in the vent region where some initial refinement has been imposed. Two levels of refinement beyond the initial coarse mesh are allowed.

Fig. 3 shows colour plots of X_{lg} , the mass fraction of light oil vapour in the gas phase, and the spatial mesh at a series of output times up to 90000 seconds (approximately 25 hours). The colour scale ranges from 0.0 (red) to 0.015 (blue). In the top plot we can see the sharp decrease from the initial value of 0.015 to zero at the free surface, and then we see the clean air (zero mass fraction of light oil) being pulled in through the free surface towards the vent. The concentration front remains sharp throughout, and the ‘clean’ region maintains a value of zero, or very small negative (of the order 10^{-5}) in places. There is no overshoot or undershoot at the moving front. The mesh refinement is seen to follow the concentration gradient, with coarsening in the ‘clean’ region.

This example solution took approximately 40 minutes of CPU time on an SGI O2 workstation (180 MHZ IP32 Processor, Secondary Cache, 256 Mbytes RAM). An equivalent run with a uniform fixed mesh corresponding to the maximum level of refinement in the adaptive mesh took over 120 minutes. Adaptivity is therefore providing significant efficiency gains. Such savings in CPU time — and corresponding memory savings — will become increasingly important as problem size increases with the inclusion of more components for example.

The post-calculated Darcy velocity vectors are shown in Fig. 4 for the developed flow (there is little change in the velocity field beyond the initial start-up phase). For clarity we have shown the velocity vectors on a uniform mesh. High local velocities are seen at the corner of the cover and at the vent.

Fig. 5 shows the calculated total mass of light oil in all the phases in the (half) domain versus time. In the earlier stages the oil extraction rate is constant and hence the total mass is a linear function of time; once the cleaner air begins to meet the vent at about 60000 seconds, concentration there will fall and hence mass reduction rates are reduced.

As yet we have not taken the solution much beyond 90000 seconds of venting for two reasons. Firstly, the point source representation of the vent is questionable in the situation of varying concentration of light oil vapour in the vicinity of the vent. It is therefore intended to model the vent more realistically. The unstructured non-uniform mesh will allow us to resolve the small scale flow in this region. Secondly, the boundary conditions at the free surface are rather crude at this stage, and the imposition of zero concentration along the whole of the top boundary is inconsistent with the small flow of vapour out of the domain in the region

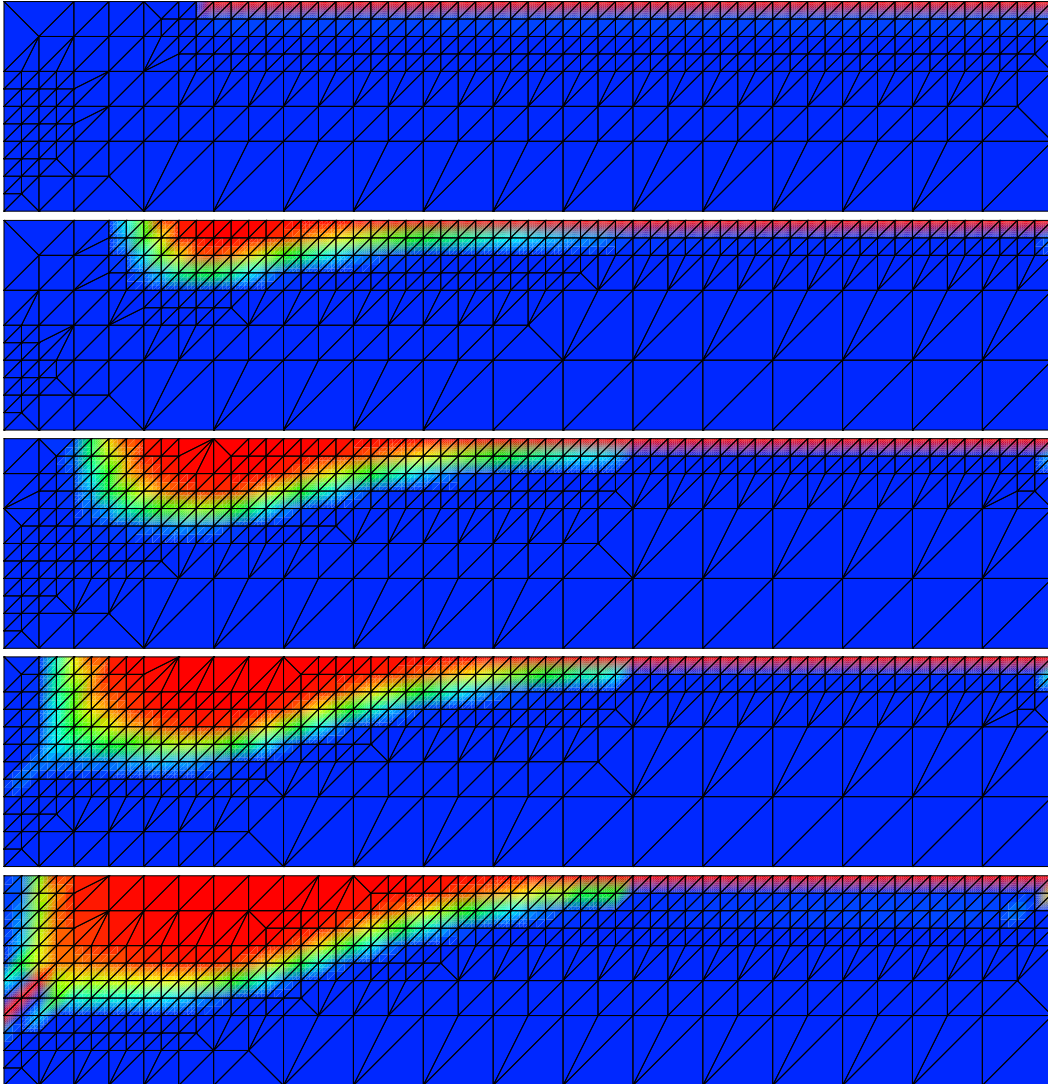


Figure 3: Colour plots of X_{lg} and the mesh at approximate output times (from the top) of 10 s, 20000 s, 40000 s, 60000 s, 90000 s

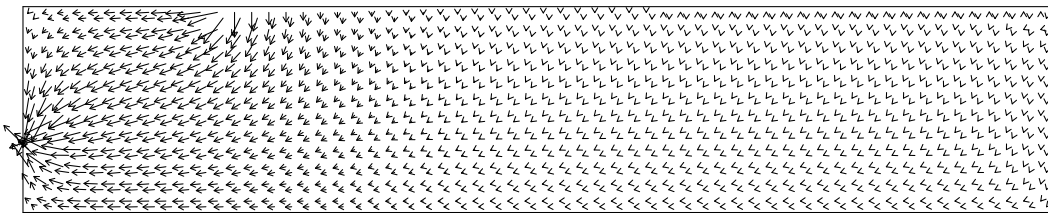


Figure 4: Velocity field (uniform mesh)

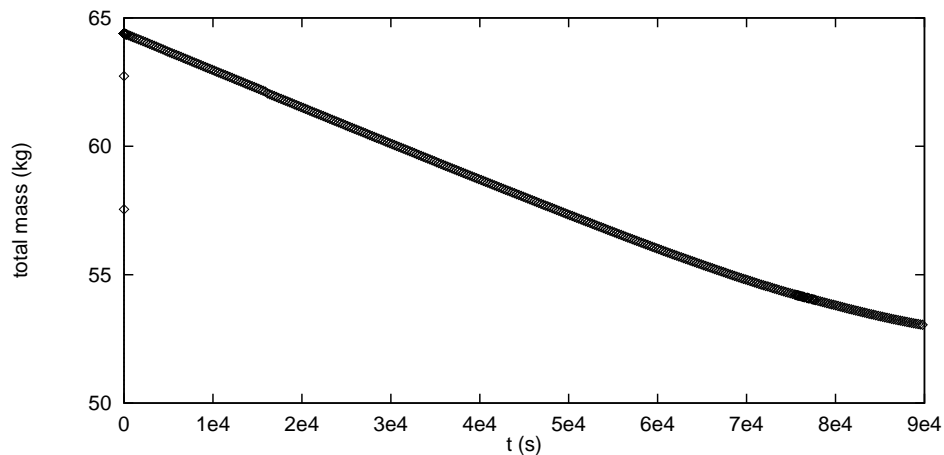


Figure 5: Total mass of light oil in the domain vs. time

not influenced by the vent, due to the high concentration gradients there. Consequently we see a peaking of the concentration just inside the free surface. Further work is required to establish how best to handle the somewhat conflicting boundary condition requirements in the inflow and outflow regions of the free surface, the extents of which are unknown a priori.

In addition to resolving the above issues, planned extensions include the incorporation of more oleic components and multiple vents, and simultaneous biodegradation processes.

Acknowledgements

The authors are grateful to Shell Research Ltd., Thornton, for sponsoring this work.

References

- [1] M. Berzins, S.V. Pennington, P.R. Pratt and J.M. Ware. *SPRINT2D software for convection dominated PDEs*. In Modern Software Tools in Scientific Computation (ed. E. Arge *et al*), Birkhauser, pp. 63–80, 1997.
- [2] M.Y. Corapcioglu and S. Panday. *Compositional multiphase flow models*. In Advances in Porous Media Volume 1 (ed. M.Y. Corapcioglu), Elsevier, pp. 1–59, 1991.
- [3] P.A. Forsyth and B.Y. Shao. *Numerical simulation of gas venting for NAPL site remediation*. Adv. Water Resources, 14, pp. 354–367, 1991.
- [4] P. Hansbo and C. Johnson. *Adaptive streamline diffusion methods for compressible flow using conservation variables*. Computer Methods in Applied Mechanics and Engineering, 87, pp. 267–280, 1991.
- [5] S.V. Pennington and P.K. Jimack. *Adaptive Numerical Simulation of the Remediation of Soil Contamination by In-Situ Gas Venting*. School of Computer Studies Research Report 98.05, University of Leeds, 1998.
- [6] F. Shakib, T.J.R. Hughes and Z. Johan. *A new finite element formulation for computational fluid dynamics: X. The compressible Euler and Navier-Stokes equations*. Computer Methods in Applied Mechanics and Engineering, 89, pp. 141–219, 1991.